JOC The Journal of Organic Chemistry

pubs.acs.org/joc Article

DFT Study on the Mechanism of 4,4′-Bipyridine-Catalyzed Nitrobenzene Reduction by Diboron(4) Compounds

Jian-Qing Qi and Lei Jiao*

Cite This: J. Org. Chem. 2020, 85, 13877−13885 Read Online

ACCESS | Metrics & More | Article Recommendations | Supporting Information

ABSTRACT: Diboron(4) compounds serve as useful reagents for borylation, diboration, and reduction in organic synthesis. A variety of pyridine derivatives have been found capable of activating diboron(4) compounds, and different reaction mechanisms have been identified. 4,4′-Bipyridine was found to activate diboron(4) to form *N*,*N*′-diboryl-4,4′-bipyridinylidene in 2015, and very recently, it has been found that this transformation is crucial in the 4,4′-bipyridine-catalyzed reduction of nitroarenes by bis(neopentylglycolato)diboron (B_2nep_2), which features the formation of arylnitrene intermediates. However, the mechanism of *N*,*N*′-diboryl-4,4′-bipyridinylidene formation, as well as its role in the transformation of nitroarene to arylnitrene, remains unknown. In this work, we investigated the possible pathways of this intriguing transformation and discovered several important intermediates through density functional theory (DFT) calculations. An *N*-boryl 4,4′-bipyridyl radical was found to be a crucial intermediate in both the formation of *N*,*N*′-diboryl-4,4′-bipyridinylidene and the reduction of nitroarene. A type of single-step reaction with three stages, including a dissociation and two migration steps, was identified in the generation of nitrosobenzene and its reduction. Arylnitrene formation was found to occur on a triplet potential energy surface, and an intersystem crossing was found to be important for achieving a reasonable activation energy barrier for nitrene formation. We anticipate our work to provide deeper insights into the nature of this reaction that could facilitate further rational design of pyridine- and bipyridine-based catalysts.

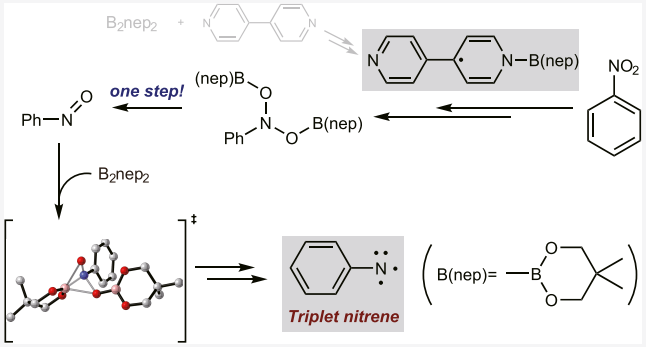

1. INTRODUCTION

Diboron(4) compounds are useful reagents in terms of both reduction and borylation, and in most cases, their application requires proper catalytic conditions to weaken or cleave the boron−boron bond.[1] Among those methods that could activate diboron(4) compounds, transition-metal-free catalytic systems have attracted much interest.[2] Recently, the utilization of azines in the activation of diboron(4) compounds has attracted much attention.

In 2015, 4,4′-bipyridine was found to display a novel behavior in activating diboron(4) compounds. It was reported that 4,4′-bipyridine can be "inserted" into the boron−boron bond to generate *N*,*N*′-diboryl-4,4-bipyridinylidene (Scheme 1a).[3] However, the mechanism of the insertion process is still unknown to date. 4-Cyanopyridine was reported to evoke direct homolytic cleavage of the boron−boron bond and form a pyridine-boryl stabilized radical complex (Scheme 1b),[4] which can subsequently be used as an equivalent of a boron radical for later borylation and diboration, or be used as a catalyst in perfluoroalkylative pyridylation of alkenes.[5] It was reported that isoquinolines could undergo stereospecific coupling with diboron(4) compounds,[6] and density functional theory (DFT) calculations revealed that this reaction proceeded through a [3,3]-sigmatropic rearrangement,[7] which corresponds to the formation of the C−C bond and dissociation of the B−B bond. By using chiral diboron compound, this reaction could be used to construct asymmetric coupling of isoquinoline derivatives (Scheme 1c).[6] 4-(4-Cyanophenyl)pyridine was found to activate diboron(4) through a [3,3]-sigmatropic rearrangement and a subsequent homolytic cleavage (Scheme 1d), forming a pyridine-boryl radical, which can be utilized as a catalyst for the reductive coupling of aldehydes.[8] Diboron(4) can also form an electron-rich borate complex when treated with 4-phenylpyridine and MeOK, which served as an electron donor to initiate the radical reaction in the borylation of aryl halides.[9] Further experimental and DFT studies revealed that the mechanism was rather distinct from that of 4-cyanopyridine.[10] In this reaction, both 4-phenylpyridine and methoxide anion worked cooperatively to promote the heterolytic cleavage of the boron−boron bond in the diboron(4) compound, which

Received: August 13, 2020
Published: October 28, 2020

https://dx.doi.org/10.1021/acs.joc.0c01963
J. Org. Chem. 2020, 85, 13877−13885

Scheme 1. Methods for the Activation of Diboron(4) Compounds by Azines

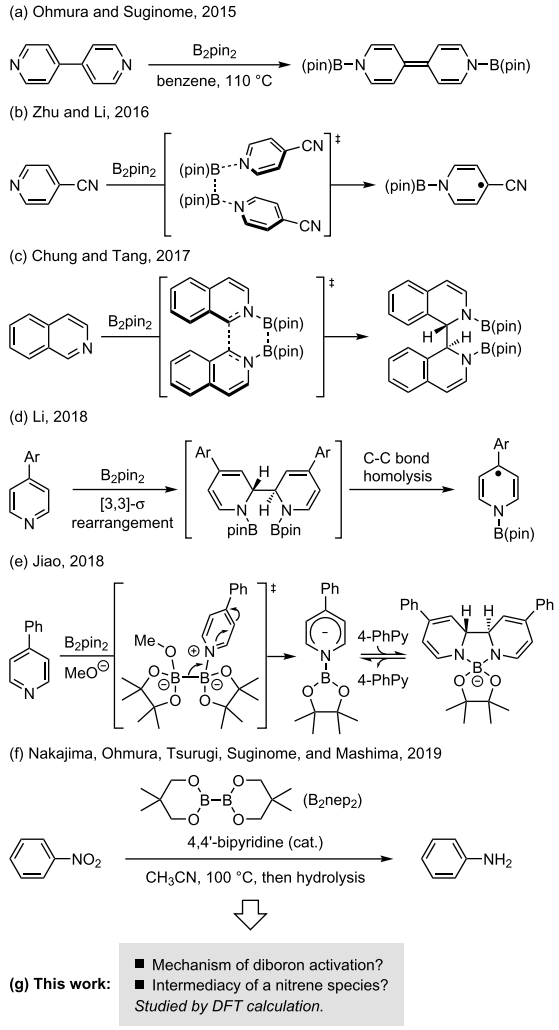

resulted in a boryl−pyridine anion complex and then afforded a 2,2′-tetrahydrobipyridine borate complex after trapping another pyridine (Scheme 1e).[10] All of the works above demonstrated various applications and great potentials of the azine-promoted diboron activation system. The nature of different reaction systems led to a variety of intriguing reaction modes and mechanisms.

Very recently, it has been reported that under the catalysis of 4,4′-bipyridine, diboron(4) compounds are capable of reducing nitroarenes to aminoarenes (Scheme 1f).[11] This reaction featured the intermediacy of the *N*,*N*′-diboryl-4,4-bipyridinylidene reported previously, and in particular, the identification of arylnitrene as a key intermediate during the reduction of nitroarene. These interesting features of the reaction were confirmed by a series of control experiments, but the detailed reaction mechanism remained elusive.[11] We envisaged that understanding the reaction mechanism would provide valuable information on the reaction and help to develop this process into a general protocol for nitrene formation from nitro compounds. Herein, we report our investigation into the mechanism of using DFT computation.

2. RESULTS AND DISCUSSION

Previous studies[3,11] have confirmed several important intermediates of the 4,4′-bipyridine-catalyzed reduction of nitrobenzene by bis(neopentylglycolato)diboron (B_2nep_2) and have subsequently deduced a preliminary mechanism of this reaction (Scheme 2).

Scheme 2. Preliminary Mechanism Proposed in Previous Studies

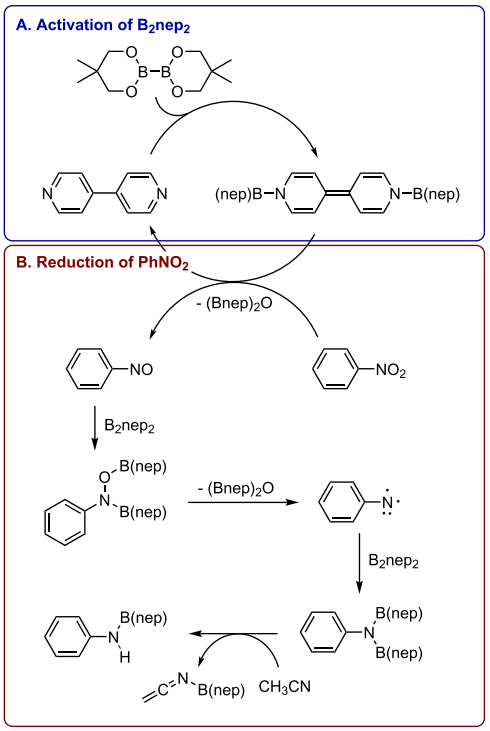

However, no mechanistic details were given in the previous works, and the pathways for both diboron(4) activation and nitroarene reduction were unclear. To better understand this reaction, two key issues need to be addressed:

1. The mechanism of diboron activation that leads to the formation of *N*,*N*′-bis-[(neopentylglycolato) boryl]-4,4′-bipyridinylidene (**3**).
2. The detailed pathway for nitrobenzene reduction, especially that for nitrene generation.

In this work, the reduction of nitrobenzene by bis(neopentylglycolato)diboron (B_2nep_2) catalyzed by 4,4′-bipyridine was chosen as the model reaction. The mechanism of the two key stages of this reduction, the activation of B_2nep_2 (Scheme 2A) and the reduction of $PhNO_2$ (Scheme 2B), was modeled by DFT calculations. The results are presented below.

2.1. Activation of Diboron(4) Compounds. Previous studies have established two different modes for the azine-promoted diborone(4) activation: direct homolysis and [3,3]-sigmatropic rearrangement/homolytic cleavage. For comparison, both pathways in the reaction between 4,4′-bipyridine and B_2nep_2 were calculated (Scheme 3).

First, we studied the direct hemolysis pathway, which mimics the mechanism of diboron(4) activation by 4-cyanopyridine.[4] In this pathway, diboron(4) coordinated with two molecules of 4,4′-bipyridine to form intermediate **14**, and then the direct homolytic cleavage of the B−B bond proceeded through **15-TS-**

https://dx.doi.org/10.1021/acs.joc.0c01963
J. Org. Chem. 2020, 85, 13877−13885

Scheme 3. Potential Energy Surface for the Formation of Radical 18

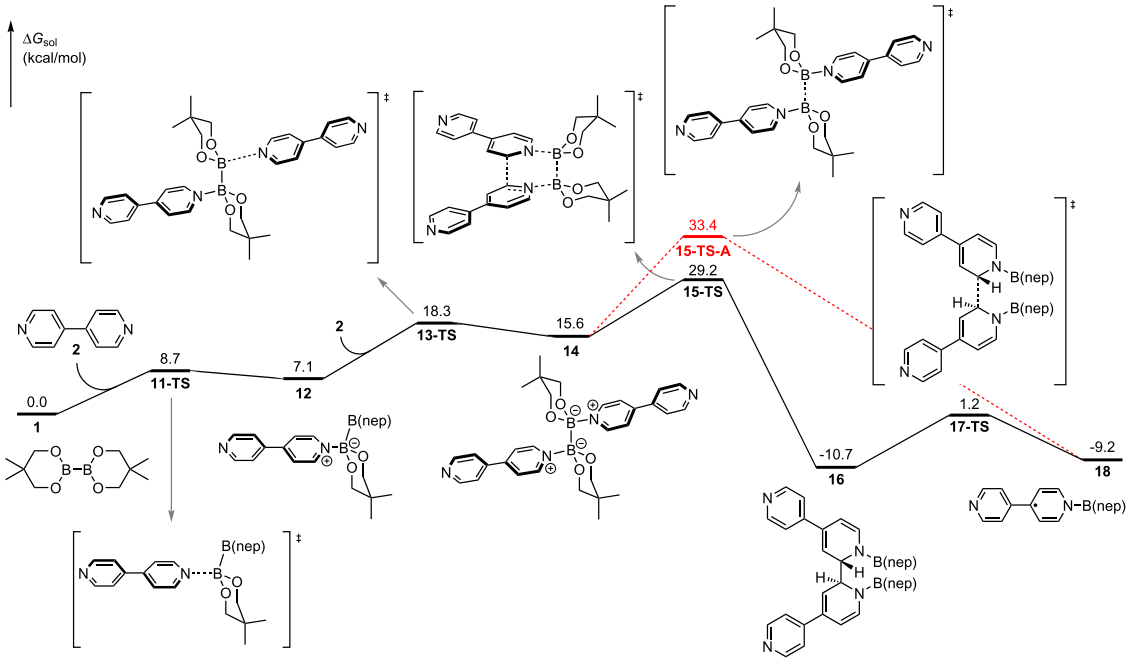

A to form two radical species **18**. The formation of adduct **14** is endergonic by 15.6 kcal/mol, and the homolytic cleavage required an overall activation free energy barrier of 33.4 kcal/mol (Scheme 3, red pathway), which made the direct homolytic pathway improbable even at 100 °C.

In the second pathway, intermediate **14** undergoes a [3,3]-sigmatropic rearrangement to form intermediate **16**, which then undergoes a C−C bond cleavage to form **18** (Scheme 3, black pathway). This pathway is similar to diboron(4) activation by either isoquinoline[6] or 4-arylpyridine.[10] DFT calculations showed that the [3,3]-sigmatropic rearrangement of **14** proceeded smoothly via **15-TS**, with an overall activation energy barrier of 29.2 kcal/mol. Compared with the direct cleavage pathway ($\Delta G^{\ddagger}_{sol}$ = 33.4 kcal/mol), the [3,3]-sigmatropic rearrangement/homolysis pathway is more reasonable.

Subsequently, radical species **18** could proceed through a chain transfer process with 4,4′-bipyridine-diboron(4) complex **12** to produce 4,4′-bipyridinylidene **3** (Scheme 4).

First, the other *N*-site of radical **18** coordinated to the vacant boron atom in **12** to form **19**. Then, the boron−boron bond in **19** cleaved homolytically to generate product **3** and release another molecule of radical **18**, which could participate in another cycle of chain transfer. The activation energy barrier of this reaction was 27.1 kcal/mol, which was kinetically more favorable than the initiation step.

It is notable that the formation of radical **18** from complex **14** was relatively slow ($\Delta G^{\ddagger}_{sol}$ = 29.2 kcal/mol). In fact, this process could be viewed as a radical initiation step that provided initial radical species **18** to facilitate the following chain transfer process. In the chain transfer process, formation of bipyridinylidene **3** and regeneration of radical **18** could proceed at a reasonable speed at 100 °C ($\Delta G^{\ddagger}_{sol}$ = 27.1 kcal/mol), and the radical chain mechanism predominated the formation of **3** from B_2nep_2 and 4,4′-bipyridine.

Finally, we found that the termination step of this radical chain process was the intermolecular reaction of two molecules of radical species **18**. Dimerization of radical **18** occurred first to

Scheme 4. Chain Transfer Mechanism for the Generation of 3

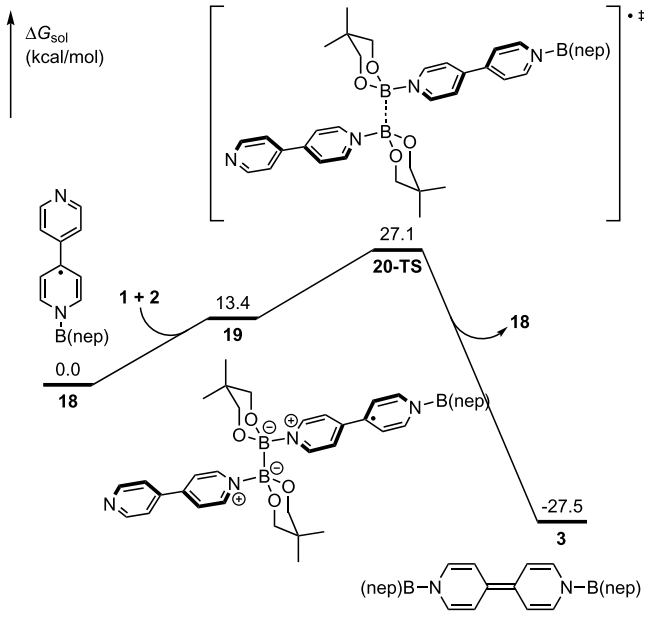

form complex **23** with a very low energy barrier, and finally, 4,4′-bipyridine dissociated from complex **23** to generate **3** (Scheme 5).

This chain termination process exhibits a low activation energy barrier ($\Delta G^{\ddagger}_{sol}$ = 2.2 kcal/mol) due to its nature of radical recombination. It is also noteworthy that its reverse process (i.e., **3** + **2** → 2 × **18**) has a reasonable activation energy barrier ($\Delta G^{\ddagger}_{sol}$ = 19.1 kcal/mol), which makes the reverse reaction viable when other reactions are draining intermediate **18**.

The three aforementioned pathways together form the full radical chain mechanism of the activation of diboron(4) compounds by 4,4′-bipyridine (Scheme 6). In the beginning, radical intermediate **18** is generated at a relatively low rate, which initiates the chain reaction. The chain transfer process

https://dx.doi.org/10.1021/acs.joc.0c01963
J. Org. Chem. 2020, 85, 13877−13885

Scheme 5. Chain Termination Mechanism

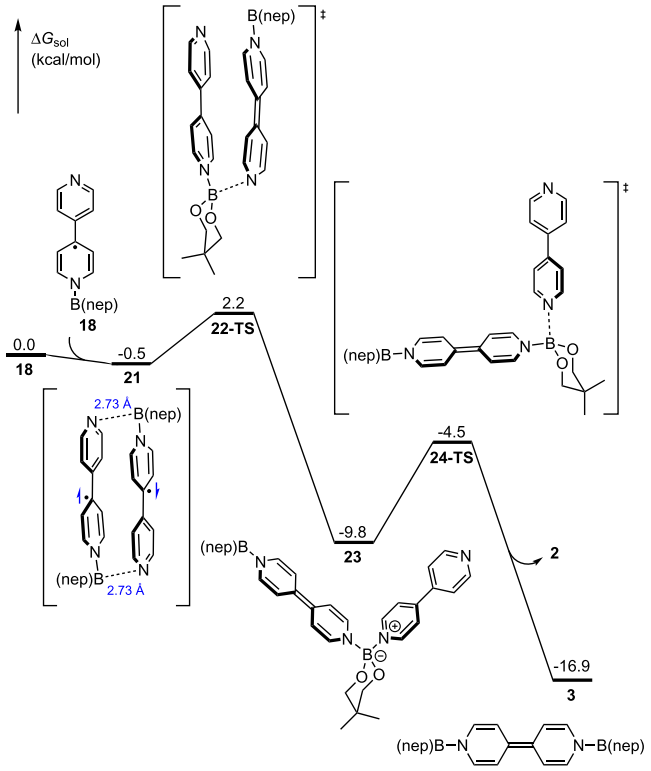

then enables the rapid formation of **3** from diboron(4) and bipyridine in the presence of **18**. The chain termination process contributes little to the generation of intermediate **3** but enables **3** to serve as a "reservoir" of radical species **18** when other reactions that consume **18** are present.

2.2. Reduction of Nitrobenzene. In this section, the mechanism of the reduction of nitrobenzene (corresponds to Scheme 2B) and how it was validated are depicted in detail.

Reduction of Nitrobenzene to Nitrosobenzene. As verified by the experimental study, in the first stage, nitrobenzene was reduced to nitrosobenzene by compound **3**. A plausible mechanism would be that nitrobenzene directly reacts with intermediate **3** to form a complex in which the oxygen atom of the nitro group is coordinated to the boryl moiety.

However, we failed to locate any of the possible complexes on the potential energy surface (PES). Meanwhile, no suitable transition state (TS) of direct boryl substitution was found.

Considering that in the presence of 4,4′-bipyridine, intermediate **3** can transform back to radical **18**, a mechanism based on the reaction between nitrobenzene and radical **18** was proposed (Scheme 7). The radical species **18** could combine with nitrobenzene, generating a new radical intermediate **25**. Intermediate **25** then underwent ligand dissociation, releasing 4,4′-bipyridine and affording radical **27**. Subsequently, radical **27** combined with another equivalent of intermediate **18** to generate **28**, which subsequently gave out 4,4′-bipyridine and compound **30**. Through relaxed PES scanning, no obvious TS for the generation of **25** and **28** was found under the current computational level.

It is noteworthy that the formation of nitrosobenzene (**5**) from intermediate **30** proceeded through only one TS (**31-TS**). In an attempt to unveil the nature of this process, we calculated the intrinsic reaction coordinate (IRC) of this reaction, analyzed the wavefunction of every geometry on the IRC, and plotted the

Scheme 6. Overview of the Mechanism of the Activation of B_2nep_2

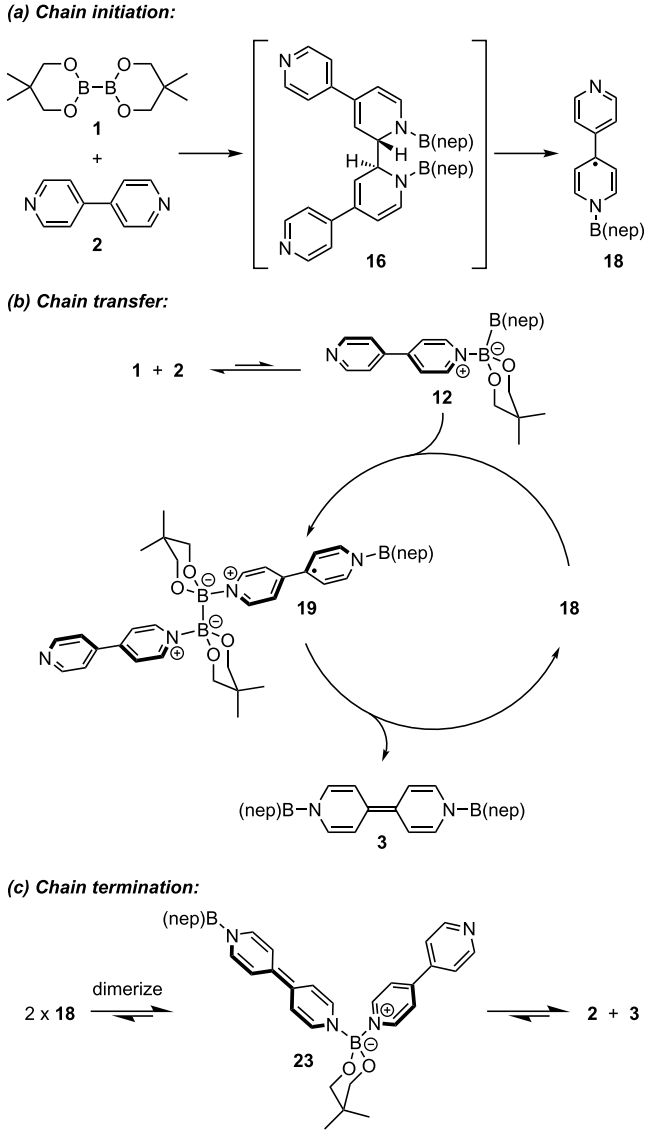

changes in the Mayer bond order of the bonds altered alongside the reaction (Figure 1, for a detailed analysis of the bond order, see Figure S2).

It was found that the reaction can be roughly divided into three stages. The first stage is the migration of the Bnep group from O1 to N. The second stage is the migration of the OBnep group from N to B1. The last stage is the heterolytic cleavage of the N–B1 bond. This process mimics a *syn*-elimination of $(Bnep)_2O$ from intermediate **30** that forms nitrosobenzene.

From Nitrosobezene to Nitrene. In the previous experiments,[11] nitrosobenzene was found able to directly react with B_2nep_2 under room temperature and form intermediate **7**, which can then transform into nitrene at 100 °C. Therefore, the formation and further transformations of intermediate **7** are critical steps of the whole reaction.

Our calculation revealed that similar to the transition between intermediate **30** and nitrosobenzene, the transition between nitrosobenzene and intermediate **7** was also a single-step reaction with one TS, **32-TS** (Scheme 8).

By calculating the IRC and analyzing each geometry on the IRC, it was found that this reaction could also be divided into

https://dx.doi.org/10.1021/acs.joc.0c01963
J. Org. Chem. 2020, 85, 13877−13885

Scheme 7. Reduction from Nitrobenzene to Nitrosobezene

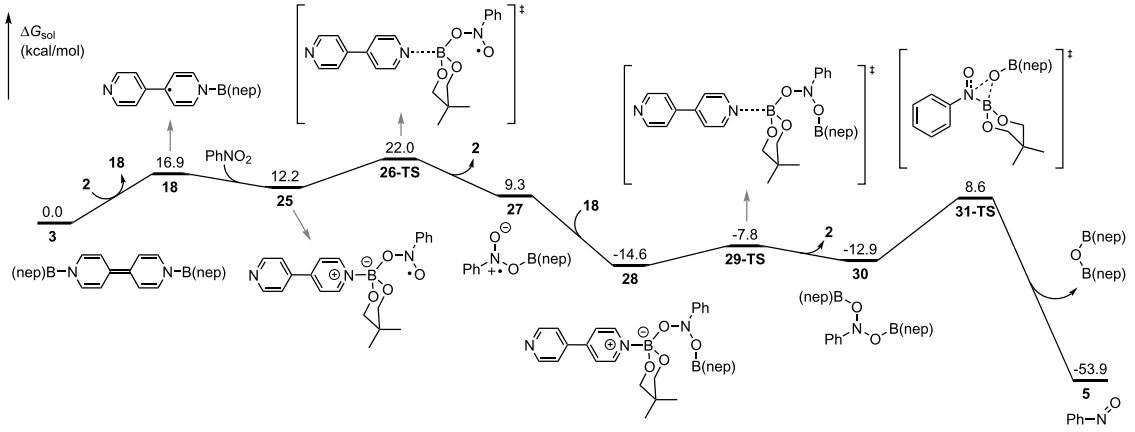

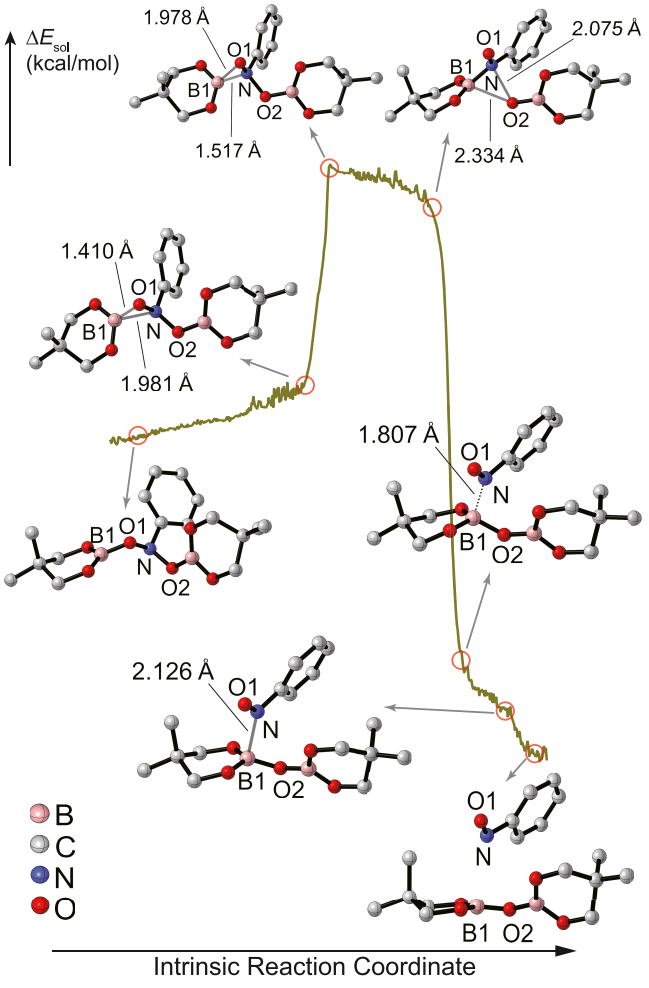

Figure 1. Analysis of the transition state **31-TS** leading to nitrosobenzene.

three stages (Figure 2, for a detailed analysis of the bond order, see Figure S3).

The first stage is the simple addition of nitrosobenzene and B_2nep_2, forming a N−B1 bond of moderate strength. The second stage is the migration of the Bnep group (containing B2) from B1 to N. In this stage, the bond length of B1−B2 increases and the bond length of N−B2 decreases. The last stage is the migration of the other Bnep group (containing B1) from N to O1. In this stage, the bond length of N−B1 increases and the

Scheme 8. From Nitrosobezene to Intermediate 7

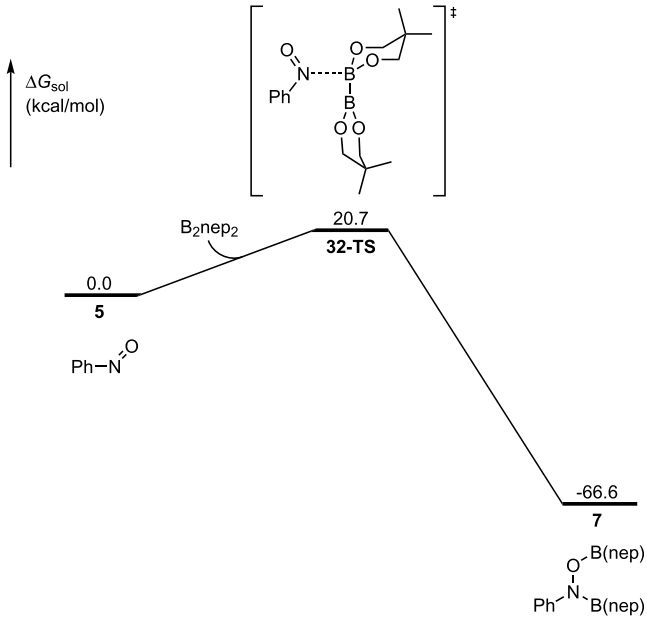

bond length of O1−B1 decreases. The whole process mimics a formal *syn*-addition of B_2nep_2 to nitrosobenzene that forms intermediate **7** in the end.

A previous study employing isolated intermediate **7** supported the existence of phenylnitrene during the reaction, as *N*,*N*-diethyl-3*H*-azepin-2-amine, the trapping product of arylnitrene, was detected in the trapping experiment with diethylamine.[11] We proposed an intramolecular elimination mechanism that rationalizes the formation of phenylnitrene from intermediate **7**. First, the transition state **33-TS** was found, which corresponds to the rearrangement of intermediate **7** to an unstable linear intermediate **34** with an activation free energy of 30.7 kcal/mol (Scheme 9). Natural population analysis revealed that the natural charge of nitrogen in **34** (−0.41391) was very close to that of the nitrogen in **7** (−0.42679). However, the natural charge of the para (−0.00903) and ortho (−0.07128 and −0.04540) carbons on the arene group in **34** is significantly more positive than that in **7** (para: −0.28068, ortho: −0.28027 and −0.29270), indicating that the positive charge was mainly distributed on the para and ortho carbons in **34**.

It was expected that by elimination of $(Bnep)_2O$, intermediate **34** could undergo a heterolytic N−B bond cleavage to afford

https://dx.doi.org/10.1021/acs.joc.0c01963
J. Org. Chem. 2020, 85, 13877−13885

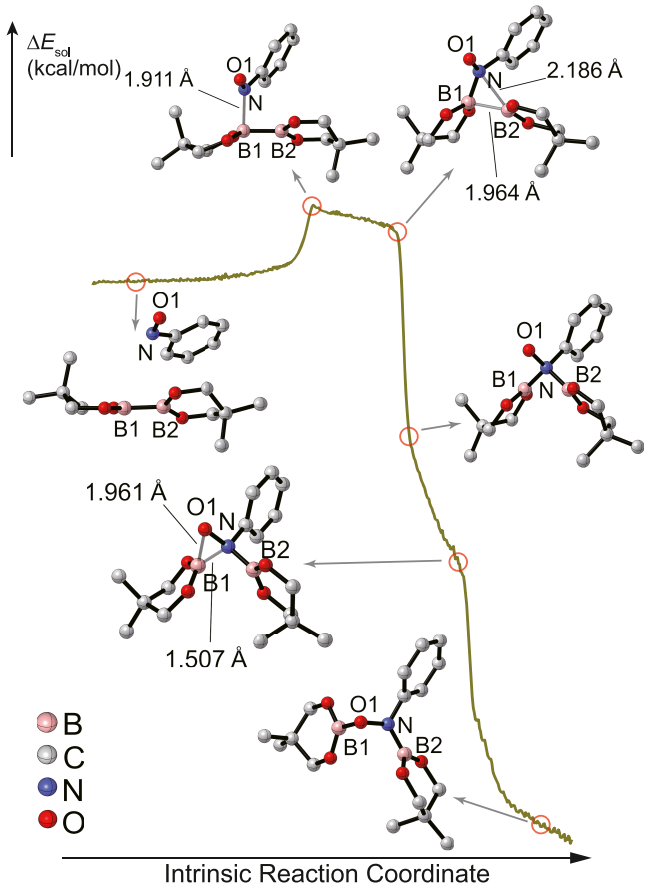

Figure 2. Analysis of the transition state **32-TS** leading to intermediate 7.

singlet phenylnitrene (**8**). However, this pathway requires an overall activation energy of 38.0 kcal/mol, making it not operable even at 100 °C (Scheme 9, red pathway).

Inspired by the intersystem crossing (ISC) of singlet nitrene,[12,13] we envisaged that intermediate **34**, a precursor of nitrene that resembles nitrene in structure, might also be able to go through an ISC and transform into its corresponding triplet state. To evaluate the possibility of this process, the minimum energy crossing point (MECP) between the singlet and triplet PESs was located (Figure 3). The electronic energy barrier of this process is only 3.1 kcal/mol, which makes ISC viable. A

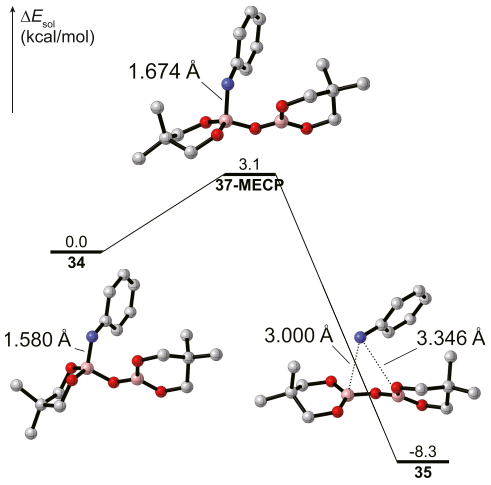

Figure 3. Minimum energy crossing point (MECP) between the singlet and triplet PESs.

rough estimation of the ISC rate was also carried out, with an estimation of estimated k_{ISC} of 4.6×10^4 s^{-1}.

The Mayer bond order analysis of intermediate **35** revealed that the Mayer bond order of the two N−B bonds are 0.03921 and 0.01007, respectively, indicating that intermolecular interactions are the main forces that drag two fragments together. Energy decomposition analysis of intermediate **36** was carried out through SAPT (Table 1), and the results showed that

Table 1. Energy Decomposition Analysis of Intermediate 35

components	electrostatics	exchange	induction	dispersion	total
E_{int}^{SAPT0} (kcal/mol)	−7.3	15.4	−2.0	−12.6	−6.5

two fragments in intermediate **35** were mainly drawn together by dispersion, indicating that intermediate **35** is, in nature, a weakly bound complex of triplet nitrene and $(Bnep)_2O$.

After the ISC, intermediate **35** can then be dissociated into triplet nitrene and $(Bnep)_2O$ via **36-TS** with a rather low activation energy barrier.

Scheme 9. Generation of Nitrene

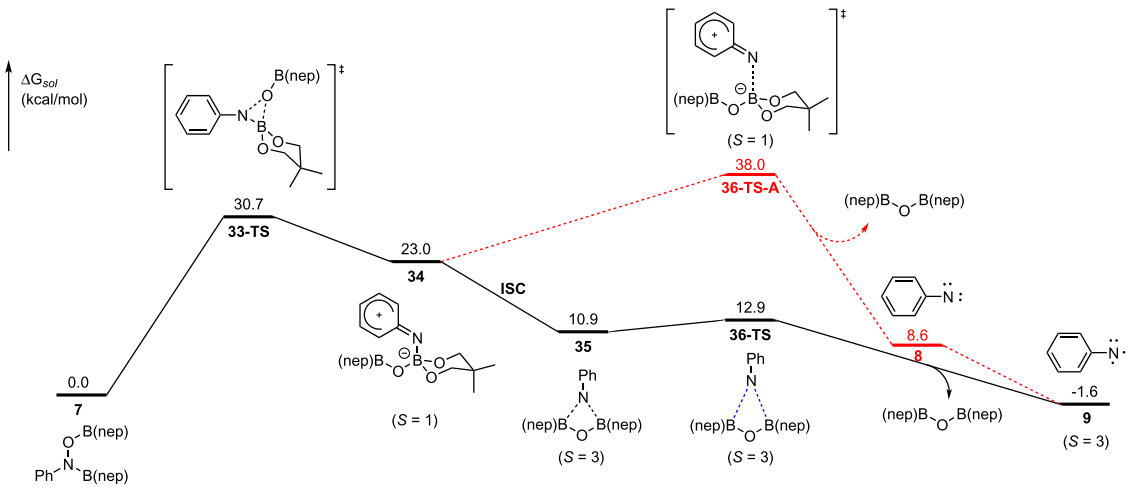

https://dx.doi.org/10.1021/acs.joc.0c01963
J. Org. Chem. 2020, 85, 13877−13885

Scheme 10. Identification of Nitrene and Later Reactions

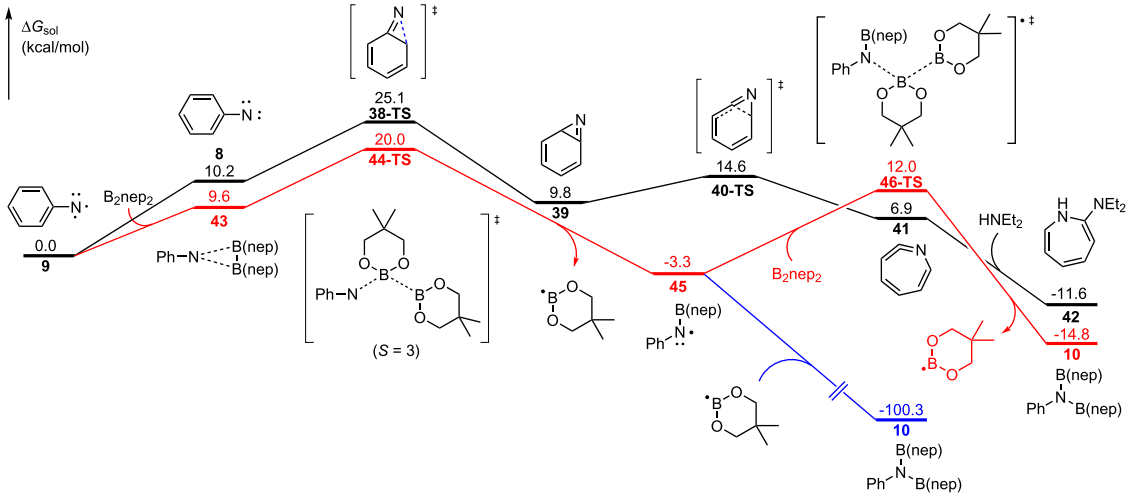

The reaction mechanism studied by DFT calculations was in agreement with the experimental findings. The original report showed that this reaction was carried out under 100 °C and could not proceed under room temperature. This phenomenon was in agreement with our DFT calculations that the highest activation barrier of this reaction was 30.7 kcal/mol (the conversion from **7** to **34**). On the other hand, the experimental fact that the reaction between nitrosobenzene and B_2nep_2 stops at intermediate **7** under room temperature[11] implied that the rate-limiting step of the reaction was after the formation of **7**, which was also the case in the DFT-modeled mechanistic pathway.

Further Reactions of Nitrene. With a reasonable pathway for nitrene formation from nitrobenzene in mind, we further studied the possible transformations of phenylnitrene that led to the production of either aniline or the trapping product.

The formation of aniline from phenylnitrene served as the major pathway in the reaction system (Scheme 10, red pathway). When excess diboron(4) existed, triplet nitrene **9** could react with it to form a triplet intermediate **43**, which was then transformed into two radicals: intermediate **45** and ·Bnep. Intermediate **45** could further combine with ·Bnep to form *N*,*N*-diborylaniline (**10**), but due to the low concentration of both radicals, this pathway might not be the major contributor to the generation of **10**. On the other hand, the interaction between **45** and another equivalent of diboron(4) became viable to form **10** via **46-TS** with a reasonable activation barrier. Upon aqueous workup, compound **10** would form aniline as the final product. It is notable that a direct "addition-type" TS leading to **10** from nitrene **8** and B_2nep_2 could not be located. Overall, the reaction leading to the formation of compound **10** was actually the reduction of phenylnitrene by diboron(4), which takes place rather rapidly under reaction conditions due to an overall activation free energy of 20.0 kcal/mol.

The experimental study showed that the phenylnitrene intermediate could also be trapped before its reduction. Compound **42**, the diethylamine capture product of ring expansion intermediate **41**, was obtained and regarded as direct evidence for nitrene formation in the reaction. We tried to figure out the detailed pathway for its formation and found that the ring expansion occurred on the singlet potential energy surface. Triplet nitrene **9** first underwent an intersystem crossing to singlet nitrene **8**. Considering the rate constant of the singlet to triplet ISC of $k_{ISC} = 3.2 \times 10^6\ s^{-1}$,[13] the rate of its reverse process was calculated to be $k_{rISC} = 2.4\ s^{-1}$, implying that this reverse ISC process is kinetically feasible. Singlet nitrene **8** subsequently underwent a three-membered ring formation via **38-TS** to intermediate **39** to generate seven-membered azine intermediate **41**. When diethylamine is present, intermediate **41** could be trapped to form intermediate **42** as the final product.[11]

It is notable that the reduction of the nitrene intermediate proceeded much more rapidly than the rearrangement, as demonstrated by the activation barriers of the two pathways (20 vs 25.1 kcal/mol). Therefore, under the catalytic reduction conditions (i.e., in the presence of excess B_2nep_2), only the reduction product was observed. Once intermediate **7** was isolated and independently reacted under elevated temperature, the products related to nitrene could be obtained.

Comparison of the Reactivity Difference between B_2nep_2 and B_2pin_2. In the preliminary research paper, it was reported that B_2nep_2 served as a suitable reductant to reduce nitroarenes under 4,4′-bipyridine catalysis, while B_2pin_2 exhibited significantly diminished reactivity.[11] We sought to understand this difference by DFT calculations according to the established mechanistic model (for details, see Schemes S1−S3 in the Supporting Information).

It was found that the formation of *N*,*N*′-diboryl-4,4′-bipyridinylidene from B_2pin_2 and 4,4′-bipyridine was viable, which was even more favorable than the reaction employing B_2nep_2 with regard to chain initiation and propagation processes (Table 2). This was consistent with the experimental findings that 4,4′-bipyridines reacted smoothly with B_2pin_2 to form *N*,*N*′-diboryl-4,4′-bipyridinylidenes. The difference was in the chain termination step, in which the B_2pin_2-related system exhibited a greater activation free energy barrier as well as an enhanced thermodynamic driving force. Since the subsequent reduction of

Table 2. Comparison of the Reactivity Difference between B_2nep_2 and B_2pin_2

energies	reaction employing B_2nep_2		reaction employing B_2pin_2	
(kcal/mol)	$\Delta G^{\ddagger}_{sol}$	ΔG_{sol}	$\Delta G^{\ddagger}_{sol}$	ΔG_{sol}
chain initiation	29.2	−9.2	26.7	−5.1
chain propagation	27.1	−27.5	27.0	−23.6
chain termination	2.7	−16.9	4.5	−18.5

https://dx.doi.org/10.1021/acs.joc.0c01963
J. Org. Chem. 2020, 85, 13877−13885

nitroarene relied on the regeneration of radical **18** from **3** (i.e., the reverse reaction of the chain termination step), this difference made the radical-generation process of the B_2pin_2-related system disfavored both kinetically and thermodynamically. Therefore, the low reactivity of B_2pin_2 in bipyridine-catalyzed nitroarene reduction could be attributed to this factor.

3. CONCLUSIONS

In this work, the mechanism of 4,4′-bipyridine-catalyzed reduction of nitrobenzene by B_2nep_2 was studied in detail by DFT calculations. We found that an important radical intermediate **18** was first generated through a [3,3]-sigmatropic rearrangement and a subsequent homolytic cleavage, which then participated in the formation of boryl bipyridinylidene intermediate **3** through a radical chain mechanism. Intermediate **3** served as a stable reservoir of **18** and nitrobenzene could react with radical **18** to finally form intermediate **30**. Intermediate **30** afforded nitrosobenzene through a complicated single-step reaction to eliminate $(Bnep)_2O$. Similarly, nitrosobenzene and B_2nep_2 were found to form intermediate **7** through a single-step reaction. Intermediate **34**, coming from the migration of **7**, could go through an ISC and transform into triplet intermediate **35**, which could generate triplet nitrene through a simple dissociation process. When diboron(4) is present, triplet nitrene can form subsequent products, otherwise, it can undergo other nitrene-related reactions. We believed that our results can evoke rational designs of new pyridine catalysts by providing deeper insights into this type of reaction, which may broaden the usage of this methodology.

4. EXPERIMENTAL SECTION

Geometry optimization and frequency calculations were carried out with Gaussian 16[14] at the M06-2X[15]/def2-SVP[16] level of theory. Single point energies were obtained at the PWPB95[17]/def2-TZVPP[16] level with DFT-D3 dispersion correction[18,19] using ORCA.[20,21] The SMD solvation model[22] was applied to all types of calculations mentioned above. The optimization of the MECP structure and the prediction of the intersystem crossing (ISC) rate were completed with ORCA[20,21] at the ωB97M-D3(BJ)[23]/def2-TZVPP[16] level. All calculations performed with ORCA were completed with RI approximation[24] and Mayer bond order[25] analysis was completed with Multiwfn.[26] The full intrinsic reaction coordinate (IRC) was computed at the B3LYP[27]/def2-SVP[16] level[28] with DFT-D3 dispersion correction[18,19] and the SMD solvation model.[22] Natural population analysis was completed with the NBO3 program.[29−33] Molecular visualization was completed with CYLview.[34] Symmetry-adapted perturbation theory[35] (SAPT) was utilized to analyze weak interactions using Psi4[36] at the level of SAPT0[37]/aug-cc-pVDZ.[38,39]

■ ASSOCIATED CONTENT

Supporting Information

The Supporting Information is available free of charge at https://pubs.acs.org/doi/10.1021/acs.joc.0c01963.

Input parameters of quantum chemistry programs used in this article; energies of all structures; and imaginary frequencies of transition states (PDF)

Cartesian coordinates of intermediates and transition states (XYZ)

■ AUTHOR INFORMATION

Corresponding Author

Lei Jiao − *Center of Basic Molecular Science (CBMS), Department of Chemistry, Tsinghua University, Beijing 100084, China;* orcid.org/0000-0002-8465-1358; Email: leijiao@mail.tsinghua.edu.cn

Author

Jian-Qing Qi − *Center of Basic Molecular Science (CBMS), Department of Chemistry, Tsinghua University, Beijing 100084, China;* orcid.org/0000-0001-5042-6315

Complete contact information is available at: https://pubs.acs.org/10.1021/acs.joc.0c01963

Notes

The authors declare no competing financial interest.

■ ACKNOWLEDGMENTS

The National Natural Science Foundation of China (Grant Nos. 21822304 and 21772110) is acknowledged for financial support. The CBMS and the Tsinghua Xuetang Program are acknowledged for providing computational resources. We also appreciate Fei-Yu Zhou and Yu-Hua Guo for inspiring discussions.

■ REFERENCES

(1) Bonet, A.; Pubill-Ulldemolins, C.; Bo, C.; Gulyás, H.; Fernández, E. Transition-Metal-Free Diboration Reaction by Activation of Diboron Compounds with Simple Lewis Bases. *Angew. Chem., Int. Ed.* **2011**, *50*, 7158−7161.

(2) Cid, J.; Gulyás, H.; Carbó, J. J.; Fernández, E. Trivalent boron nucleophile as a new tool in organic synthesis: reactivity and asymmetric induction. *Chem. Soc. Rev.* **2012**, *41*, 3558.

(3) Ohmura, T.; Morimasa, Y.; Suginome, M. Organocatalytic Diboration Involving "Reductive Addition" of a Boron−Boron −Bond to 4,4-Bipyridine. *J. Am. Chem. Soc.* **2015**, *137*, 2852−2855.

(4) Wang, G.; Zhang, H.; Zhao, J.; Li, W.; Cao, J.; Zhu, C.; Li, S. Homolytic Cleavage of a B—B Bond by the Cooperative Catalysis of Two Lewis Bases: Computational Design and Experimental Verification. *Angew. Chem., Int. Ed.* **2016**, *55*, 5985−5989.

(5) Cao, J.; Wang, G.; Gao, L.; Chen, H.; Liu, X.; Cheng, X.; Li, S. Perfluoroalkylative pyridylation of alkenes via 4-cyanopyridine-boryl radicals. *Chem. Sci.* **2019**, *10*, 2767−2772.

(6) Chen, D.; Xu, G.; Zhou, Q.; Chung, L. W.; Tang, W. Practical and Asymmetric Reductive Coupling of Isoquinolines Templated by Chiral Diborons. *J. Am. Chem. Soc.* **2017**, *139*, 9767−9770.

(7) Zhou, Q.; Tang, W.; Chung, L. W. Mechanistic insights into asymmetric reductive coupling of isoquinolines by a chiral diboron with DFT calculations. *J. Organomet. Chem.* **2018**, *864*, 97−104.

(8) Cao, J.; Wang, G.; Gao, L.; Cheng, X.; Li, S. Organocatalytic reductive coupling of aldehydes with 1,1-diarylethylenes using an in situ generated pyridine-boryl radical. *Chem. Sci.* **2018**, *9*, 3664−3671.

(9) Zhang, L.; Jiao, L. Pyridine-Catalyzed Radical Borylation of Aryl Halides. *J. Am. Chem. Soc.* **2017**, *139*, 607−610.

(10) Zhang, L.; Jiao, L. Super electron donors derived from diboron. *Chem. Sci.* **2018**, *9*, 2711−2722.

(11) Hosoya, H.; Misal Castro, L. C.; Sultan, I.; Nakajima, Y.; Ohmura, T.; Sato, K.; Tsurugi, H.; Suginome, M.; Mashima, K. 4,4-Bipyridyl-Catalyzed Reduction of Nitroarenes by Bis(neopentylglycolato)diboron. *Org. Lett.* **2019**, *21*, 9812−9817.

(12) Young, M. J. T.; Platz, M. S. Mechanistic analysis of the reactions of (pentafluorophenyl)nitrene in alkanes. *J. Org. Chem.* **1991**, *56*, 6403−6406.

(13) Gritsan, N. P.; Zhu, Z.; Hadad, C. M.; Platz, M. S. Laser Flash Photolysis and Computational Study of Singlet Phenylnitrene. *J. Am. Chem. Soc.* **1999**, *121*, 1202−1207.

(14) Frisch, M. J.; Trucks, G. W.; Schlegel, H. B.; Scuseria, G. E.; Robb, M. A.; Cheeseman, J. R.; Scalmani, G.; Barone, V.; Petersson, G. A.; Nakatsuji, H.; Li, X.; Caricato, M.; Marenich, A. V.; Bloino, J.; Janesko, B. G.; Gomperts, R.; Mennucci, B.; Hratchian, H. P.; Ortiz, J. V.; Izmaylov, A. F.; Sonnenberg, J. L.; Williams; Ding, F.; Lipparini, F.;

Egidi, F.; Goings, J.; Peng, B.; Petrone, A.; Henderson, T.; Ranasinghe, D.; Zakrzewski, V. G.; Gao, J.; Rega, N.; Zheng, G.; Liang, W.; Hada, M.; Ehara, M.; Toyota, K.; Fukuda, R.; Hasegawa, J.; Ishida, M.; Nakajima, T.; Honda, Y.; Kitao, O.; Nakai, H.; Vreven, T.; Throssell, K.; Montgomery Jr., J. A.; Peralta, J. E.; Ogliaro, F.; Bearpark, M. J.; Heyd, J. J.; Brothers, E. N.; Kudin, K. N.; Staroverov, V. N.; Keith, T. A.; Kobayashi, R.; Normand, J.; Raghavachari, K.; Rendell, A. P.; Burant, J. C.; Iyengar, S. S.; Tomasi, J.; Cossi, M.; Millam, J. M.; Klene, M.; Adamo, C.; Cammi, R.; Ochterski, J. W.; Martin, R. L.; Morokuma, K.; Farkas, O.; Foresman, J. B.; Fox, D. J. *Gaussian 16*, Rev. A.03; Wallingford, CT, 2016.

(15) Zhao, Y.; Truhlar, D. G. The M06 suite of density functionals for main group thermochemistry, thermochemical kinetics, noncovalent interactions, excited states, and transition elements: two new functionals and systematic testing of four M06-class functionals and 12 other functionals. *Theor. Chem. Acc.* **2008**, *120*, 215−241.

(16) Eichkorn, K.; Weigend, F.; Treutler, O.; Ahlrichs, R. Auxiliary basis sets for main row atoms and transition metals and their use to approximate Coulomb potentials. *Theor. Chem. Acc.* **1997**, *97*, 119−124.

(17) Goerigk, L.; Grimme, S. Efficient and Accurate Double-Hybrid-Meta-GGA Density Functionals−Evaluation with the Extended GMTKN30 Database for General Main Group Thermochemistry, Kinetics, and Noncovalent Interactions. *J. Chem. Theory Comput.* **2011**, *7*, 291−309.

(18) Becke, A. D.; Johnson, E. R. A density-functional model of the dispersion interaction. *J. Chem. Phys.* **2005**, *123*, No. 154101.

(19) Johnson, E. R.; Becke, A. D. A post-Hartree-Fock model of intermolecular interactions: Inclusion of higher-order corrections. *J. Chem. Phys.* **2006**, *124*, No. 174104.

(20) Neese, F. The ORCA program system. *Wiley Interdiscip. Rev.: Comput. Mol. Sci.* **2012**, *2*, 73−78.

(21) Neese, F. Software update: the ORCA program system, version 4.0. *Wiley Interdiscip. Rev.: Comput. Mol. Sci.* **2018**, *8*, No. e1327.

(22) Marenich, A. V.; Cramer, C. J.; Truhlar, D. G. Universal Solvation Model Based on Solute Electron Density and on a Continuum Model of the Solvent Defined by the Bulk Dielectric Constant and Atomic Surface Tensions. *J. Phys. Chem. B* **2009**, *113*, 6378−6396.

(23) Najibi, A.; Goerigk, L. The Nonlocal Kernel in van der Waals Density Functionals as an Additive Correction: An Extensive Analysis with Special Emphasis on the B97M-V and B97M-V Approaches. *J. Chem. Theory Comput.* **2018**, *14*, 5725−5738.

(24) Weigend, F.; Häser, M.; Patzelt, H.; Ahlrichs, R. RI-MP2: optimized auxiliary basis sets and demonstration of efficiency. *Chem. Phys. Lett.* **1998**, *294*, 143−152.

(25) Mayer, I. Charge, bond order and valence in the AB initio SCF theory. *Chem. Phys. Lett.* **1983**, *97*, 270−274.

(26) Lu, T.; Chen, F. Multiwfn: A multifunctional wavefunction analyzer. *J. Comput. Chem.* **2012**, *33*, 580−592.

(27) Stephens, P. J.; Devlin, F. J.; Chabalowski, C. F.; Frisch, M. J. Ab Initio Calculation of Vibrational Absorption and Circular Dichroism Spectra Using Density Functional Force Fields. *J. Phys. Chem. A* **1994**, *98*, 11623−11627.

(28) We tried to calculate the IRC at the original level, but failed to get the full IRC. We thought that it was because the PES at the original level has a very flat region. Therefore, another level was used, see Supporting Information for detailed analysis.

(29) Foster, J. P.; Weinhold, F. Natural hybrid orbitals. *J. Am. Chem. Soc.* **1980**, *102*, 7211−7218.

(30) Reed, A. E.; Weinhold, F. Natural bond orbital analysis of near-Hartree−Fock water dimer. *J. Chem. Phys.* **1983**, *78*, 4066−4073.

(31) Reed, A. E.; Weinstock, R. B.; Weinhold, F. Natural population analysis. *J. Chem. Phys.* **1985**, *83*, 735−746.

(32) Reed, A. E.; Weinhold, F. Natural localized molecular orbitals. *J. Chem. Phys.* **1985**, *83*, 1736−1740.

(33) Carpenter, J.; Weinhold, F. Analysis of the geometry of the hydroxymethyl radical by the "different hybrids for different spins" natural bond orbital procedure. *THEOCHEM* **1988**, *169*, 41−62.

(34) Legault, C. Y. CYLview. http://www.cylview.org 2009.

(35) Jeziorski, B.; Moszynski, R.; Szalewicz, K. Perturbation Theory Approach to Intermolecular Potential Energy Surfaces of van der Waals Complexes. *Chem. Rev.* **1994**, *94*, 1887−1930.

(36) Parrish, R. M.; et al. Psi4 1.1: An Open-Source Electronic Structure Program Emphasizing Automation, Advanced Libraries, and Interoperability. *J. Chem. Theory Comput.* **2017**, *13*, 3185−3197.

(37) Gonthier, J. F.; Sherrill, C. D. Density-fitted open-shell symmetry-adapted perturbation theory and application to π-stacking in benzene dimer cation and ionized DNA base pair steps. *J. Chem. Phys.* **2016**, *145*, No. 134106.

(38) Dunning, T. H. Gaussian basis sets for use in correlated molecular calculations. I. The atoms boron through neon and hydrogen. *J. Chem. Phys.* **1989**, *90*, 1007−1023.

(39) Kendall, R. A.; Dunning, T. H.; Harrison, R. J. Electron affinities of the first-row atoms revisited. Systematic basis sets and wave functions. *J. Chem. Phys.* **1992**, *96*, 6796−6806.

https://dx.doi.org/10.1021/acs.joc.0c01963
J. Org. Chem. 2020, 85, 13877−13885